Pu Coexists in Three Oxidation States in a Borosilicate Glass: Implications for Pu Solubility

Sebastian Bahl,[†] Sylvain Peuget,[§] Ivan Pidchenko,[†] Tim Pruessmann,[†,⊥] Jörg Rothe,[†] Kathy Dardenne,[†] Julien Delrieu,[§] David Fellhauer,[†] Christophe Jégou,[§] Horst Geckeis,[†] and Tonya Vitova*[,†]

[†]Institute for Nuclear Waste Disposal, Karlsruhe Institute of Technology, P.O. Box 3640, 76021 Karlsruhe, Germany

[§]Institut de Chimie Séparative de Marcoule, CEA Valrhô Marcoule, UMR 5257, BP 17171, 30207 Bagnols sur Cèze, France

ABSTRACT: Pu(III), Pu(IV), and a higher oxidation state of Pu, likely Pu(VI), are for the first time characterized simultaneously present in a borosilicate glass using Pu M_5 edge high energy resolution X ray absorption near edge structure (HR XANES) technique. We illustrate that the method can be very efficiently used to determine Pu oxidation states, which control the solubility limit of Pu in a glass matrix. HR XANES results show that the addition of excess Si_3N_4 is not sufficient for complete reduction of Pu to Pu(III), which has a relatively high solubility limit (9−22 wt % Pu) due to its network modifying behavior in glasses. We provide evidence that the initially added Pu(VI) might be partly preserved during vitrification at 1200/1400 °C in Ar atmosphere. Pu(VI) could be very advantageous for vitrification of Pu rich wastes, since it might reach solubility limits of 40 wt % comparable to U(VI).

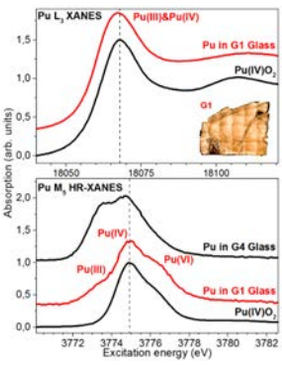

INTRODUCTION

High level nuclear waste with low Pu content is typically generated from reprocessing of commercial spent nuclear fuel (SNF) and is commonly immobilized in glass matrices. Borosilicate glass is most often applied, for example, in France, United States, India, and UK.[1−4] The quantity of Pu is well below 1 wt % in these waste glass products and Pu management is of less consideration compared to highly radioactive fission products and volatile (e.g., Cs and Tc) as well as low soluble (e.g., Mo, Pt, Ru, etc.) constituents of SNF. Pu enriched defense waste and Pu waste obtained from reprocessing of SNF is of high concern and requires tailored immobilization strategies.[5] Waste products of chemically and microstructurally homogeneous nature are often an essential requirement for its safe long term disposal in an underground nuclear waste repository. Beside crystalline ceramics, borosilicate glasses are also discussed as appropriate matrices.[6] However, formation of separate phases heterogeneously distributed in the glass can lead to differential swelling and/or poor leaching performance in a worst case scenario of groundwater intrusion.[7,8] The Pu solubility is restricted to a few weight percent in most common glasses. Vienna et al. composed an aluminosilicate glass, which is able to incorporate up to 11 wt % of PuO_2 in its matrix.[9] A higher Pu loading was only reported by Feng et al.[10] By reducing Pu to its trivalent state during vitrification, an equivalent to 10−25 wt % PuO_2 was homogeneously incorporated in a glass matrix without forming any Pu rich agglomerates. This study illustrates that not only the glass composition but even to higher extent the oxidation state of Pu is the crucial factor for the Pu solubility in glass matrices. Likewise Schreiber and Balazs demonstrated that up to 40 wt % U(VI) can be incorporated, whereas the solubility limit for U(IV) does not exceed 9 wt %.[11] This behavior can be explained by the mechanism describing the accommodation of the actinide (An) elements in the glass network. Depending on their oxidation state, the An can play the role of either network forming or network modifying elements, and thereby their solubility limits can be greatly variable.[12,13] Deschanels et al. concluded that the way of incorporation can be predicted for all cations according to their charge and distance to the next oxygen atoms (Dietzel's field strength).[8] The Pu(III) resembles the network modifying elements, while the Pu(IV) species has more a network forming behavior.

Tailored glass compositions and vitrification processes leading to desired oxidation states of the An elements require sensitive characterization methods. One of the widely used tools for determination of the oxidation states of the An elements is the An L_3 edge X ray absorption near edge structure (XANES) technique. However, because of the large spectral $2p_{3/2}$ core hole lifetime broadening contributing to the An L_3 edge XANES (7.8 eV),[14] the spectrum is insensitive to the presence of minor amounts of An oxidation states.[15,16] Deschanels et al. studied the Pu solubility in borosilicate glass and prepared several homogeneous glasses with increasing Pu content (0.85−8 wt % PuO_2) and variable amount of reducing agent.[8] They characterized the Pu oxidation state by the Pu L_3 edge XANES technique and reported stabilization of Pu in its

tetra and trivalent oxidation states. We reexamined the oxidation states of Pu in the same glass samples reported by Deschanels et al. applying the more advanced Pu M_5 edge high energy resolution XANES (HR XANES) method. The An $M_{4,5}$ HR XANES technique recently emerged as a valuable direct probe of the An 5f valence orbitals, which are largely responsible for the chemical bonding in the An compounds.[17−23] It was demonstrated that the spectra are very sensitive to the An oxidation states and allow, for example, to distinguish between U(IV), U(V), and U(VI) species when mixed in the same material, not easily possible with other spectroscopy techniques.[16,20,24] This method probes the bulk of the material (1 μm penetration depth) and does not require vacuum conditions as, for example, the laboratory based surface sensitive X ray photoelectron spectroscopy (1−10 nm penetration depth). Because of the drastically reduced core hole lifetime broadening (~0.5 eV)[23] contributing to the spectrum compared to the Pu L_3 absorption edge (7.8 eV)[14] and the improved experimental energy resolution, the spectral resolution is significantly enhanced, providing more reliable access to the An oxidation states.

We provide new insights into the redox behavior of Pu, which controls the solubility of Pu in glass matrices. The Pu oxidation state and its local atomic environment, probed with Pu L_3 edge EXAFS, are correlated to the applied vitrification conditions and the added amount of reducing agent. The first application of the Pu M_5 edge HR XANES technique for oxidation states characterization of Pu with the specific example of Pu incorporated into borosilicate glasses is reported. We demonstrate the need for development and application of such advanced methods for investigations of complex nuclear waste products.

EXPERIMENTAL SECTION

Preparation of Samples. The Pu doped glasses were synthesized in the Atalante laboratories of the *Commissariat à l'énergie atomique et aux énergies alternatives* (CEA) Marcoule Centre, France. The chemical composition of the Pu glass and the preliminary structural analyses can be found in the publication by Deschanels et al.[8] Two different base glass compositions were used for the synthesis. For the glasses, molten at reducing conditions (G2−G4, cf. Table 1b), a simplified composition was used instead of the complex composition applied for the G1 glass (cf. Table 1a) to minimize potential impact of additional elements on the Pu solubility. As the simplified composition contains the major constituents of the complex composition, both glasses are considered to be structurally similar. This was additionally shown by molecular dynamics calculations.[25] Pu 239 oxide (cf. Table S1) dissolved in 1.6 M nitric acid solution under aerobic conditions was added to the glass frit before melting. No redox state adjustment and no redox state analysis was performed for the Pu solutions. Reducing conditions were obtained by adding Si_3N_4 for the G2−G4 samples (cf. Table 2). *R* corresponds to the quantity of Si_3N_4 used in relation to the amount of Pu. It was experimentally optimized by Cachia et al., who studied the reduction of Ce(IV) to Ce(III) in the same glass and synthesis conditions but without HNO_3 feeding.[26] A theoretical *R* value of 0.07 did not yield any Ce(III).

Table 1. Glass Frit Compositions Used to Vitrify Pu[8]

(a) complex composition (wt %)

SiO_2	45 46	Li_2O	2	Cs_2O	1
B_2O_3	14 15	Fe_2O_3	3	BaO	0.5 0.6
Na_2O	10 11	MoO_3	2 3	SrO	0.3 0.4
Al_2O_3	5	ZrO_2	2 3	REE oxides	3 4
CaO	4	ZnO	2 3	other oxides	2 3

(b) simplified composition (wt %)

SiO_2	59	Al_2O_3	4.3	ZnO	3.2
B_2O_3	18	CaO	5.2	ZrO_2	0.7
Na_2O	7	Li_2O	2.6		

Table 2. Fabrication Characteristics of Pu Doped Glasses; $R = m(Si_3N_4)/m(PuO_2)$

sample	melting temperature (°C)	PuO_2 (wt %)	atmosphere	crucible	*R*
G1	1200	0.85	Ar	Pt	0
G2	1400	2.0	Ar	Pt	0.37
G3	1400	4.0	Ar	Pt	0.56
G4	1400	8.0	Ar	Pt	0.73

Therefore, the reducing agent was applied with threefold excess obtaining predominantly Ce(III). For application to the Pu glass the required amount was calculated and increased by 50%. It is listed along with the Pu loading in Table 2.

As the glass components are usually present as oxides, their concentrations are given as common oxide compounds, notwithstanding the fact that the element might be present in another oxidation state (e.g., Pu is not necessarily present as Pu(IV) in the glasses). The four Pu doped glass samples G1−G4 were mounted in a Plexiglas cell equipped with Kapton windows with 13 and 8 μm thickness serving as inner and outer containment, respectively (cf. Figure S1).

The $Pu(IV)O_2$ reference sample for HR XANES measurements was prepared as follows: PuO_2 powder was filled in the hole of a stainless steel washer with 15 mm diameter, which was glued on a Kapton tape. Washer and PuO_2 powder were covered with 13 μm Kapton foil and sealed with a Kapton tape. Two more washers were used to create a second independent containment by using 8 μm Kapton foil and a Kapton tape. Pu^{3+} and PuO_2^{2+} solutions (0.02 M each) were electrochemically prepared in 1 M $HClO_4/NaClO_4$ and served as reference samples for the Pu M_5 edge HR XANES/XAFS studies (denoted as $Pu(III)_{aq}$ and $Pu(VI)_{aq}$).[23,27] The Pu(III) and Pu(VI) oxidation states were confirmed (100% purity) by vis−NIR spectroscopy.

Pu M_5 Edge HR-XANES Spectroscopy. The samples were investigated at the INE Beamline and CAT ACT Beamline, KIT Synchrotron (previously ANKA), Karlsruhe Institute of Technology (KIT), Karlsruhe, Germany. The primary X ray beam was vertically collimated by a cylindrically bent Rh coated (INE Beamline)/bare Si (CAT ACT Beamline) mirror, monochromatized by a Si(111) double crystal monochromator (DCM) and focused by a toroidal double focusing Rh (INE Beamline)/Si (CAT ACT Beamline) coated mirror to an approximate 0.5 × 0.5 mm^2 beam spot onto the sample. A detailed description of the INE Beamline is reported by Rothe et al.[18] The CAT ACT Beamline is described by Zimina et al.[28,29] At both beamlines the DCMs were calibrated by assigning 3775 eV to the maximum of the most intense absorption resonance (white line, WL) of the Pu M_5 edge HR XANES spectrum of a PuO_2 reference sample. The energy calibration of the DCM has ±0.05 eV uncertainty equal to half of the energy step size. Pu M_5 edge HR XANES spectra were recorded with a multianalyzer crystals X ray emission spectrometer.[23,29−31] A gastight box enclosing the spectrometer and the sample maintaining constant He atmosphere during all measurements was installed to avoid intensity losses due to scattering and absorption of photons in the tender X ray regime. The Pu M_5 edge HR XANES spectra were obtained by recording the maximum intensity of the Pu M_α emission line (3339 eV) diffracted by the five spherically bent Si(220) crystal analyzers (Saint Gobain Crystals, France) with 1 m bending radius and focused onto a single diode VITUS Silicon Drift Detector (KETEK, Germany). The crystals were aligned at 75.22° Bragg angle. The sample, crystals, and detector were arranged in five vertical Rowland circles intersecting at the sample surface and the detector entrance window.

Pu M_5 edge HR XANES spectra were recorded with three different experimental energy resolutions denoted as "low", "medium", and "high". The $Pu(III)_{aq}$ and $Pu(VI)_{aq}$ spectra were measured at the INE Beamline with low energy resolution. The spectra of the G1−G4 glasses and the PuO_2 reference material were recorded with both medium (INE Beamline) and high (CAT ACT Beamline) experimental energy resolutions. The differences in the resolution are due to variations in the beam size on the sample and the experimental energy resolution of the DCMs at the two beamlines. To achieve the highest resolution, the beam size was confined to 500 × 500 μm size by applying a pinhole in front of the sample and additional masks giving access only to the central section of the analyzer crystals. For the medium experimental energy resolution, the full width at half maximum (fwhm) of the incident beam (3349.1 eV) elastically scattered from a Teflon sample was 1.2 ± 0.05 eV. The most intense absorption resonances of PuO_2 spectra measured with the three different experimental energy resolutions exhibit a fwhm of 3.73 (low), 3.27 (medium), and 2.73 (high resolution) eV, respectively (cf. Figure S2). Pu M_5 edge HR XANES spectra for the PuO_2 reference were measured after each Pu glass to verify the calibration of the DCM. Spectra were recorded from 3760 to 3835 eV with varying step sizes (3760−3770 eV: 0.5 eV; 3770−3790 eV: 0.1 eV; 3790−3835 eV: 0.5 eV) and 10 (medium resolution)/30 s/step (high resolution) integration time. Typically, two to three scans were collected at room temperature and averaged. All spectra were normalized to the maximum absorption intensity. The energy positions of the different absorption resonances were obtained by fitting the spectra with several Gaussian and one arctangent function. The fit was performed with the Fityk curve fitting software v.0.9.8 (http://fityk.nieto.pl/), which uses the Levenberg−Marquardt least squares algorithm (cf. Table S2). Figure S3 depicts exemplarily the G1 spectrum and its fit.

Pu L_3 Edge XAFS Spectroscopy. Pu L_3 edge X ray absorption fine structure (XAFS = EXAFS−extended X ray absorption fine structure and XANES) experiments were also performed at the INE Beamline. The DCM was equipped with two Ge(422) crystals, and the spectra were recorded in transmission detection mode using three ionization chambers filled with Ar. Zr (K edge = 17 998 eV) foil was simultaneously measured with all samples to control the energy calibration of the DCM. The energy calibration of the DCM has ±0.25 eV uncertainty equal to half of the energy step size in the XANES region. Four to six scans were collected at room temperature and averaged for each sample in the range of 17 877−19 306 eV; a 0.5 eV step size was used in the XANES region of the spectra, and equidistant k steps (0.04 $Å^{-1}$) were used in the post edge EXAFS region. The averaged Pu L_3 edge XANES scans were normalized by subtraction of a linear background function from the featureless pre edge region and normalization of the edge jump to unity. The WL energy position was obtained by determining the x axis intercept of the first derivative spectra.

The EXAFS spectra ($\chi(k)$) were extracted, Fourier transformed, and modeled using the ATHENA and ARTEMIS programs included in the IFEFFIT program package.[32] The spectra were weighted by k = 1, 2, and 3 within the k = 2.4−10.3 $Å^{-1}$ range. Hanning windows with dk = 2 $Å^{-1}$ sills were used. The fit was performed in R space for R = 1.3−2.46 Å range. The single scattering paths used in the modeling were generated with the FEFF8.2 code using the PuO_2 fluorite structure (Inorganic Crystal Structure Database (ICSD) collection code 55456).[33] The first coordination sphere was modeled by varying the distance (R(Å)) to the absorbing atom, the Debye−Waller (DW, σ^2 ($Å^2$)) factor, and the energy shift of the ionization potential (ΔE_0 (eV)), while the coordination number (N) was fixed. In a second step, the coordination number was varied simultaneously with the DW factor obtained from the first step and the energy shift, whereas the distance was fixed. The amplitude reduction factor S_0^2 was fixed to 0.9 during the fit. This value was found from modeling the EXAFS spectrum of a PuO_2 reference compound measured in the same experimental conditions.[34] The obtained goodness of fit (r factor) is 0.1% (r = 0.001) or 0.2% (r = 0.002) corresponding to the difference between data and model.

RESULTS

Pu L_3 Edge XANES. Figure 1 depicts the Pu L_3 edge XANES spectra of the Pu doped G1−G4 glass samples and the

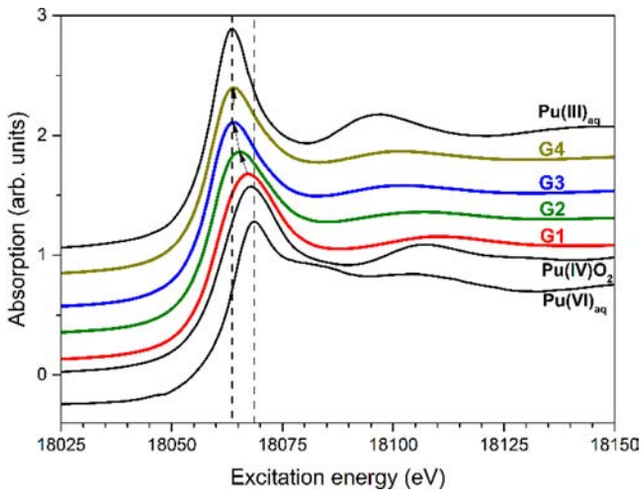

Figure 1. Pu L_3 edge XANES spectra of the G1−G4 glasses and the $Pu(III)_{aq}$, $Pu(IV)O_2$, $Pu(VI)_{aq}$ references.

$Pu(III)_{aq}$, $Pu(IV)O_2$, $Pu(VI)_{aq}$ reference materials. The Pu L_3 edge XANES spectra mainly describe dipole allowed electronic transitions from $2p_{3/2}$ to unoccupied 6d orbitals ($2p_{3/2}$→6d). The energy positions of the abrupt increase in absorption (absorption edge) and the most intense absorption resonance (white line, WL) typically shift to higher energies by reduction of the electronic density in the vicinity of the Pu atom nucleus; this energy shift of the spectrum is commonly used for oxidation state analyses. However, the spectra can also shift due to changes in the short and long range atomic environment around the absorbing atom. For example, Conradson et al. found up to 2 eV energy shift of the WLs of the Pu L_3 edge XANES spectra of several Pu(IV) materials with varying coordination environments.[34,35] A well known challenge is to differentiate between Pu(IV) and Pu(VI), where the latter tends to form short trans dioxo bonds with lengths of 1.75 Å (Pu yl, plutonyl) in both solid and liquid states.[36,37] Because of the strong covalence of the plutonyl bond, there is an accumulation of electronic charge on the Pu atoms. As a result, the $2p_{3/2}$ core hole is well screened, and the WL positions of the Pu(VI) and the Pu(IV) spectra coincide (cf. Figure 1). Note that the Pu L_3 edge XANES of Pu(V) trans dioxo species (axial bond length ∼1.94 Å) is even shifted to lower energies compared to the spectrum of Pu(IV).[35] A trend indicated with solid black arrows can be observed in the spectra in Figure 1. The energy position of the WL of the G1 spectrum is slightly shifted to lower energies compared to the WL of the Pu(IV) reference spectrum suggesting contribution of Pu(III) in the G1 sample. For R values less than 0.73 (G1−G3), mixtures of most likely tri and tetravalent Pu are formed. The energy positions of the WLs of the G4 and the Pu(III) spectra coincide suggesting efficient reduction of Pu(IV) to Pu(III) in the G4 glass caused by the reducing agent (R = 0.73; Table 2). These results are in good agreement with the report of Deschanels et al., who also applied the Pu L_3 edge XANES technique to investigate the Pu oxidation states in the glasses G1−G3.[8] However, these analyses cannot exclude potential stabilization of minor amounts of higher Pu oxidation states.

Pu M_5 Edge HR-XANES. Figure 2 depicts the Pu M_5 edge HR XANES spectra of the G1−G4 glass samples and the

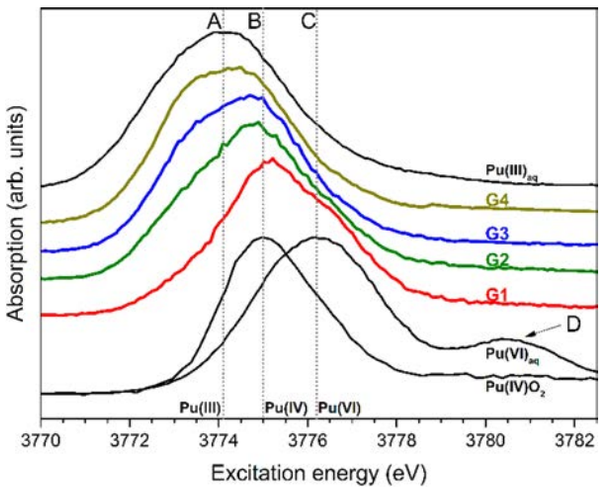

Figure 2. Pu M_5 edge HR XANES spectra of the G1−G4 glasses, $Pu(IV)O_2$ reference, and the $Pu(III)_{aq}$, $Pu(VI)_{aq}$ references recorded with medium and low experimental energy resolution, respectively.

$Pu(III)_{aq}$, $Pu(IV)O_2$, $Pu(VI)_{aq}$ reference materials. The Pu M_5 edge HR XANES spectra describe the dipole allowed transitions of $3d_{5/2}$ electrons to 5f unoccupied orbitals ($3d_{5/2}\rightarrow 5f$), which contain most of the An valence electrons participating in the chemical bonding. The valence electronic configuration of metallic Pu is $7s^25f^6$. In contrast to the Pu L_3 edge XANES spectra, the Pu M_5 edge HR XANES reference spectra clearly shift to higher energies in the order Pu(III), Pu(IV), Pu(VI); Pu(V) is difficult to stabilize; therefore, no reference spectrum is presented. The spectra of the $Pu(III)_{aq}$ and $Pu(VI)_{aq}$ references were recorded with lower experimental energy resolution. This results in a larger broadening of the spectra. Considering the PuO_2 spectra measured with variable experimental energy resolutions (cf. Figure S2) a shift toward lower energies of up to 0.1 eV can be expected for $Pu(III)_{aq}$ and $Pu(VI)_{aq}$ spectra if measured with a resolution comparable to the glass spectra. The G1 and the Pu(IV) spectra have very similar energy positions (cf. Figure 2, line B), which is a strong indication that Pu(IV) is the main species in the G1 sample. The G2−G4 spectra are shifted to lower energies with increasing *R*. The spectrum of G4 peaks at approximately the energy position of line A (3774.1 eV) marking the most intense absorption resonance of the Pu(III) reference spectrum. This general trend suggests a reduction of the Pu oxidation state going from G1 to G4 in agreement with the Pu L_3 edge results. However, the G1−G4 spectra have asymmetric shapes. There are shoulders on the low (3774.1 eV) and high (3776.5 eV) energy sides of the G1 spectrum, which increase and decrease in intensity, respectively, going from the G1 to the G4 spectrum. The energy position of the main absorption peak can vary by ca. ±0.1 eV for the same U oxidation state but different coordination environments,[16,24,38] whereas there is, for example, ∼1.50 ± 0.05 eV shift between the peaks marked with lines B and C in Figure 4. Therefore, these additional spectral features point to mixtures of Pu(III) (line A), Pu(IV) (line B), and a higher oxidation state of Pu (line C).

We recorded the G1, G4, and PuO_2 spectra with even higher experimental energy resolution. These spectra are depicted in Figure 3. The shoulder C is well pronounced in the G1

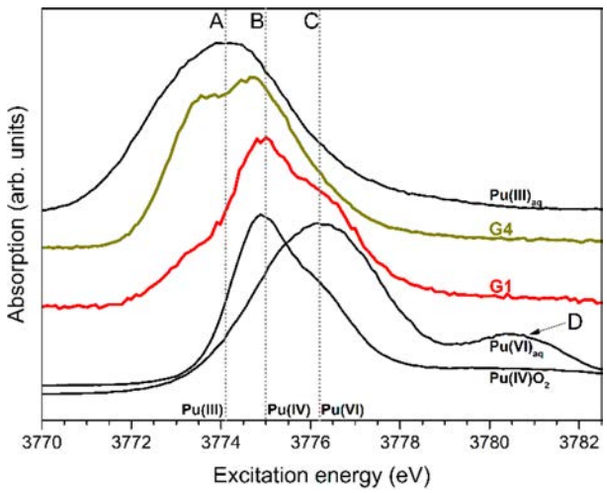

Figure 3. Pu M_5 edge HR XANES spectra of the G1, G4 glasses, $Pu(IV)O_2$ reference, and the $Pu(III)_{aq}$, $Pu(VI)_{aq}$ references recorded with high and low experimental energy resolution, respectively.

spectrum affirming the formation of Pu species with higher than IV oxidation state. The low energy shoulder corresponding to minor contribution of Pu(III) is now clearly distinguishable in the G1 spectrum. The high energy resolution enables also distinct detection of Pu(III) and Pu(IV) in the G4 glass. The spectrum demonstrates formation of similar amounts of Pu(III) and Pu(IV). As the spectra of G1 and G4 in Figure 3 were measured with a higher experimental resolution, a 0.3 eV shift of the spectra toward lower energies can be expected compared to the Pu glass spectra measured with medium experimental resolution (Figure 2). Figure S2 depicts PuO_2 spectra recorded with different resolutions from which this shift can be deduced (cf. ref 23). The shoulder marked with line C on the high energy side of the main peaks of the G1 and G2 spectra (3776.5 eV) nearly coincides with the main peak of the Pu(VI) reference. Therefore, we infer that this spectral contribution is likely due to the presence of Pu(VI) (line C). Pu(V) is less probable, but it might be potentially stabilized in the glass matrix as well; therefore, we cannot completely exclude its presence. The post edge feature D in the Pu(VI) reference spectrum is characteristic for plutonyl[22,23] and describes transitions to the sigma antibonding (σ^*) molecular orbital.[22] A similar peak was reported recently also for uranyl by Vitova et al.[22,38] As feature D is not present in the spectra of G1 and G2, we conclude that the potential Pu(VI) species does not form a plutonyl type of bonding. A spectrum of Pu(V) yl is not available, but comparing to U, the D peak should be visible in a Pu(V) yl spectrum too. Reducing U(VI) yl ($[U(VI)O_2(CO_3)_3]^{4-}$) to U(V) yl ($[U(V)O_2(CO_3)_3]^{5-}$) leads to decrease of the energy shift of the D peak with respect to the main peak maximum, but it is still well distinguishable.[27] It is more likely that the Pu−O distances are elongated and that the Pu is coordinated by a more symmetric set of O atoms than in the plutonyl case, that is, in a plutonate structure.[39] For example, Pu can form PuO_6^{n-} polyhedra with octahedral coordination of six equidistant O atoms.[40] It was previously shown that the σ^* peak is not present for U(V)/U(VI) species in U_3O_8, (U(V) and U(VI)) and U_4O_9 (U(IV) and U(V)), which are characterized by orthorhombic space group[41] and cuboctahedron coordination,[42] respectively.[20]

On the basis of these experimental evidences we conclude that Pu(IV) mainly contributes to the G1 and G2 glasses. This

finding is in good agreement with literature reporting the formation of Pu(IV) in Pu doped borosilicate glasses melted in ambient conditions without reducing agent.[26,43] Adding Si_3N_4 to the vitrification feed mixture increases significantly the Pu(III) content as previously reported.[8] Pu(III) then becomes a major constituent of the G3 and G4 glasses. When considering the redox balance of the Si_3N_4 reaction with $Pu(NO_3)_4$, the reductant is in significant excess only in sample G4. Apparently, this is not sufficient to reduce all Pu to Pu(III).

Pu L_3 Edge EXAFS Investigations. The EXAFS spectra of the G1−G4 glasses and their best fits are shown in *k* and *R* space in Figure 4. The analysis of the EXAFS region of the XAFS spectra provides quantitative information about the number and type of neighboring atoms as well as their distances to the absorbing Pu atom. The usable *k* range is restricted by a signal at ∼11 $Å^{-1}$, which results from a minor Am 241 (<0.2% of the Pu amount) contamination in the glasses. The Fourier transformed EXAFS (FT EXAFS) spectra are depicted in Figure 4b (back transformed FT EXAFS spectra cf. Figure S4). In all samples the Pu atoms are coordinated by ∼5.5 O atoms (Table 3). The average Pu−O distance, however, changes from 2.25 to 2.27 Å for samples G1 and G2 to 2.34 Å for samples G3 and G4. This trend indicates that the effective charge on the Pu atoms decreases resulting in an increased bond length. This observation can be explained by the increasing reduction of Pu within the glass series as already revealed by the XANES/HR XANES investigations. The fit results also illustrate that plutonyl bonds with lengths shorter than 1.8 Å are not obtained from the EXAFS fits, which is well in agreement with the results derived from Pu M_5 edge HR XANES. Note that the Pu(VI)−Oax bond length of plutonyl in nitric acid solution initially added is 1.68−1.71 Å.[44,45] Figure 5 and Figure 6 depicts the distribution of Pu−O bond distances for ∼100 Pu compounds reported in the ICSD. The bond lengths obtained from the fit to our spectra are indicated by arrows. Pu(IV) is likely a major constituent of G1 and G2, whereas both Pu(III) and Pu(IV) are major constituents for the G3 and G4 glasses (cf. Figure 5). It is apparent that the increase of the Pu−O bond length with 0.09 Å from G1 to G4 leads to a bond length characteristic for Pu(III) compounds. No Pu(III) compound with Pu−O interatomic distances found for the G1/G2 samples is reported in the ICSD database. The short Pu−O bond lengths typical for the Pu(VI) and Pu(V) plutonyl species are visible at less than 2 Å in Figure 6. The spectra display only one O coordination shell. Therefore, we can conclude that no Pu rich crystalline phases are formed in the glass matrix. Pu(VI) compounds forming a plutonate structure are coordinated mainly octahedrally by six O atoms with an average distance of ∼2.2−2.3 Å.[40] The finding of a Pu−O distance of 2.25 and 2.27 Å and a coordination of ∼5.5 for samples G1 and G2 agrees well with Pu−O distances in Pu(IV) compounds and with the proposed Pu(VI) formation in a plutonate type of bonding. A few Pu(V) compounds are listed in the database. The reported bond lengths are 0.17 Å longer than found for G1 and G2.

Combining the outcome of HR XANES and L_3 edge EXAFS results, we conclude that the Pu species characterized by the C feature in HR XANES should be rather assigned to Pu(VI). The impact of the U oxidation state and coordination on its final speciation in glass vitrified in Ar atmosphere was not systematically investigated.

But U(VI) nitrate solution and solid uranyl nitrate hexahydrate added to a borosilicate glass frit melted in aerobic conditions at 1300/1200 °C form U−Oax bonds with 1.82[47] and 1.84 Å[48] lengths, respectively. Those are longer than the 1.77[49]/1.75[50] Å U−Oax bond lengths for the uranyl initially added. Hence U(VI) and Pu(VI) appear to have similar behavior.

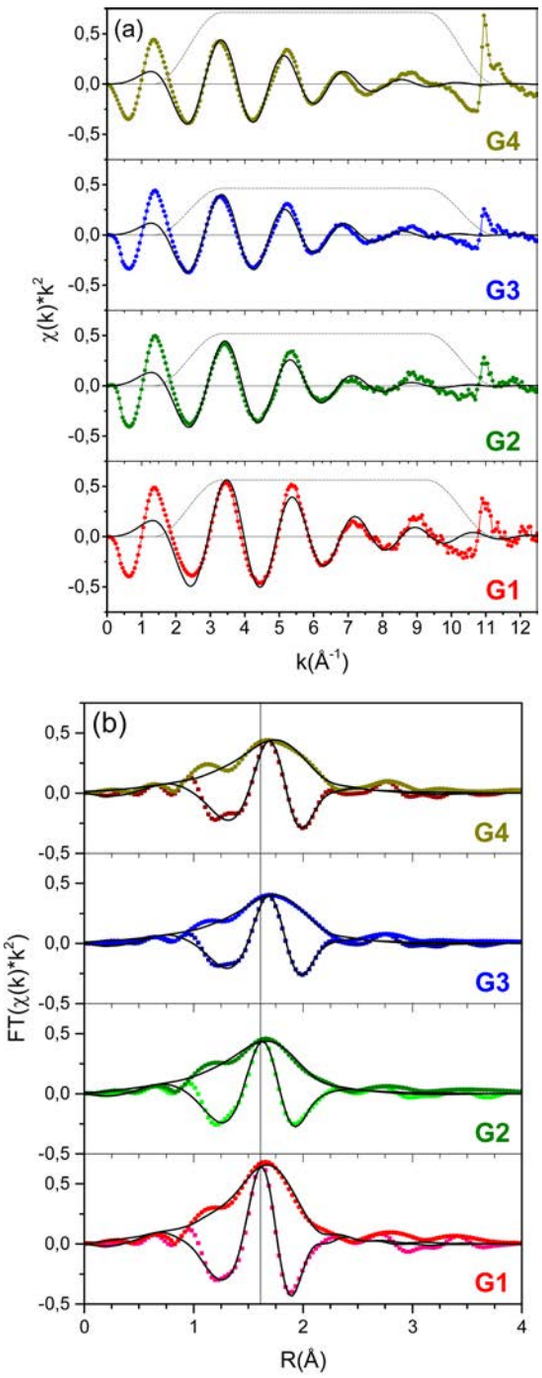

Figure 4. Pu L_3 edge $\chi(k)$ (a) and FT EXAFS (b) spectra of the G1−G4 glasses. The $\chi(k)$ (a) and the magnitude and imaginary part (b) of the experimental spectra are shown with colored symbols, whereas black lines represent fit results.

DISCUSSION

We report here for the first time that Pu(VI) can be stabilized during melting at 1200 °C (G1)/1400 °C (G2) in Ar atmosphere. Stump et al. succeeded as well to incorporate major amounts of Pu(VI) during sol−gel synthesis at 100 °C

Table 3. EXAFS Fit Results[a] for Pu Glass Samples

sample	SP	N	R (Å) ± 0.01	σ^2 (Å^2)	ΔE_0 (eV)
G1	Pu O1	5.7 ± 0.3	2.25	0.011 ± 0.001	7.2 ± 0.6
G2	Pu O1	5.7 ± 0.4	2.27	0.017 ± 0.002	7.4 ± 0.8
G3	Pu O1	5.3 ± 0.4	2.34	0.016 ± 0.001	5.7 ± 0.7
G4	Pu O1	5.8 ± 0.5	2.34	0.016 ± 0.001	5.7 ± 0.8

[a]SP—scattering path, N—coordination number, R—bond distance, σ^2—Debye—Waller factor, ΔE_0—energy shift of the ionization potential.

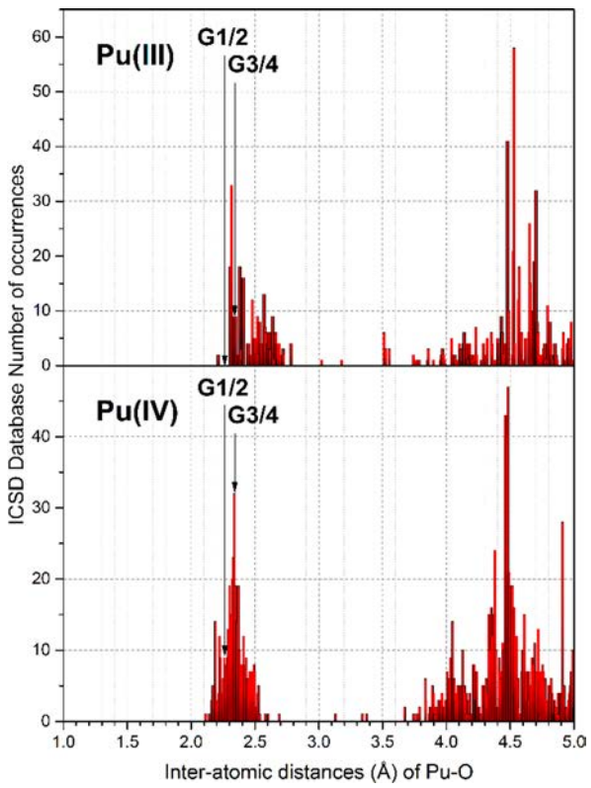

Figure 5. Statistics for Pu—O distances in Pu(III) and Pu(IV) compounds reported in the ICSD database.[46] The Pu—O distances obtained from the EXAFS fits for the G1—G4 samples are indicated with black arrows.

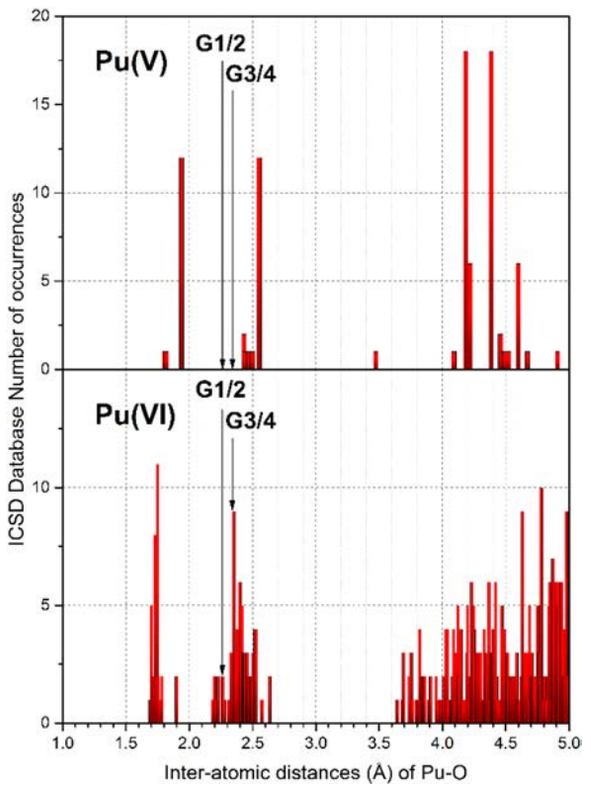

Figure 6. Statistics for Pu—O distances in Pu(V) and Pu(VI) compounds reported in the ICSD database.[46] The Pu—O distances obtained from the EXAFS fits for the G1—G4 samples are indicated with black arrows.

obtaining a glass like material.[51] However, successive heating to 800 °C completely reduced Pu(VI) to Pu(IV). UV—vis spectroscopy was applied in this study to characterize Pu oxidation states, which is, however, not very sensitive for solid materials so that minor contributions of Pu(VI) cannot be excluded. Conditions stabilizing Pu(VI) in a borosilicate glass matrix are controversially reported in the literature. Stevanovsky et al. performed in 2010 a Pu L_3 edge XAFS study and described partial Pu oxidation to Pu(VI) in a lanthanide borosilicate glass stored for more than 1.5 years in air.[52] On the contrary Hess et al. investigated 15 year old Pu doped borosilicate glass synthesized at 1200 °C with different α activities with Pu L_3 edge XAFS spectroscopy and found unaltered Pu(IV), even for high α decay accumulations from 8.8×10^{15} to 1.9×10^{18} α decays/g.[43] Our glass samples were exposed to a slightly lower dose level of 1 to 6×10^{16} α decays/g. In a similar manner, Bouty et al. studied α self irradiation effects in an eight year old Cm and Pu doped borosilicate glass synthesized at 1400 °C that accumulated ~6×10^{18} α decays/g. In agreement with Hess et al. no effect of the radiation on the tetravalent Pu oxidation state was found.[53] According to our investigations described above, it is apparent that the Pu L_3 XANES method is not sensitive to minor fractions of Pu redox species. As a result, minor Pu(V)/Pu(VI) contributions possibly could not be resolved in those previous investigations. Because of the fact that we found in our investigations Pu(VI) only in two samples, even though all four samples had the same storage and radiation exposure history, we suppose that Pu(VI) formation can be attributed to the synthesis process of the Pu doped glasses rather than to storage conditions or radiation effects. It is more likely that Pu(VI) in our experiments forms due to the vitrification of Pu dissolved in 1.6 M nitric acid. Tri , tetra , and hexavalent Pu species can be stabilized in HNO_3 solution at pH values below 2.[36,40] Despite melting under Ar atmosphere a part of Pu(VI) is apparently maintained in the glass. In case of the G1 glass sample redox active elements like Fe are present, while the G2 glass sample does not contain such components. Since both glasses show the presence of Pu(VI), those elements seem to have minor impact on the Pu speciation.[53]

Our results suggest that when Pu dissolved in nitric acid is vitrified Pu(VI) species can be stabilized in nuclear waste glass along with other Pu redox species. The Pu M_5 edge HR XANES investigations show that the increasing contribution of

Pu(III) can be correlated with the rising amount of added reducing agent. The HR XANES method illustrates that Pu(IV) still remains as the main redox species, even though Si_3N_4 is added in excess. A complete reduction to Pu(III) apparently requires the establishment of even stronger reducing conditions during the vitrification process. The observation of Pu(VI) species in the G1 and G2 glasses opens a potential doorway to incorporate Pu(VI) in a stable manner in a waste glass product, which might be of interest for designing vitrification processes for Pu rich waste. The solubility behavior of Pu(VI) in borosilicate glass has not been systematically investigated so far. But as Pu cations in low oxidation states are believed to be incorporated in glass matrices in a similar manner as other An cations (e.g., U), it can be deduced that Pu(VI) is likely well soluble in borosilicate glass. Indeed, Schreiber et al. reported a maximum U(VI) solubility in borosilicate glass of 40 wt %.[11] This would even exceed the Pu(III) solubility equivalent to 10−25 wt % PuO_2 reported by Feng et al. by far and open the opportunity to vitrify Pu rich nuclear wastes in a very efficient and economical way. Depending on the isotopic composition, the limiting factor of the Pu loading will be more likely the risk of criticality rather than its solubility in the glass matrix. The United States Department of Energy (DOE), for example, restricts its waste acceptation criteria by a very conservative limit of 987 g of fissile material per cubic meter of glass (∼0.04 wt %).[54] Criticality issues could, however, be solved by addition of neutron absorbing elements like Gd and Hf, which is foreseen for the immobilization of Pu by incorporation in ceramics.[55]

Mobilization of hexavalent Pu when the glass is in contact with solutions in a repository is certainly of less relevance. In the long term the Pu leaching rate is governed by the overall glass matrix dissolution and is independent from the Pu oxidation state.[56] The redox state of dissolved Pu species will then be determined by the given geochemical milieu and notably by the prevailing redox conditions. Despite more local oxidative redox conditions near the glass interface due to α radiolysis, usually, reducing conditions are expected due to iron canister corrosion resulting in relatively high concentrations of Fe(II) and H_2 in the leachates. Pu will most probably exist in reduced oxidation states exhibiting low solubility, strong sorption to surfaces, and potentially formation of mobile colloidal species.

CONCLUSION

The Pu M_5 edge HR XANES method is clearly capable of detecting Pu(III), Pu(IV), and likely Pu(VI) being simultaneously present in a nuclear glass sample. Quantitative analyses of the Pu species with different oxidization states are possible when spectra of appropriate reference materials are recorded under the same experimental conditions. Our study demonstrates that this characterization method can be used for monitoring the redox conditions in vitrification processes upon reductant addition. A clear correlation of Pu oxidation state distribution and added reductant amount is revealed. By partial reduction to Pu(III) the solubility of Pu in the borosilicate glass was increased to greater than 8 wt %, whereby no separated Pu rich phases could be identified. For complete reduction of Pu to the trivalent state in glass of similar chemical composition, it is necessary to add more reducing agent and to adjust R to a value higher than 0.73. This will most likely increase the Pu loading in the glass further.

We also clearly detected for the first time formation of Pu in higher than (IV) oxidation state. Pu(VI) species preserved in the glasses synthesized upon addition of a Pu solution in nitric acid is likely. Further experiments are needed to verify if Pu(VI) yields higher solubility as compared to Pu(III). In case of an analogy of Pu(VI) and U(VI) behavior in glass, a solubility limit of ∼40 wt % can be expected, which could open a new way to increase Pu solubility in glass waste forms.

AUTHOR INFORMATION

Corresponding Author

*E mail: Tonya.Vitova@kit.edu.

ORCID

Tim Pruessmann: 0000 0002 7903 9199

Tonya Vitova: 0000 0002 3117 7701

Present Address

[⊥]Karlsruhe Institute of Technology (KIT), Institute of Catalysis Research and Technology (IKFT), P.O. 3640, D 76021 Karlsruhe, Germany; Karlsruhe Institute of Technology (KIT), Institute for Chemical Technology and Polymer Chemistry (ITCP), Engesserstr. 20, D 76131 Karlsruhe, Germany

Notes

The authors declare no competing financial interest.

ACKNOWLEDGMENTS

The authors acknowledge the Helmholtz Association of German Research Centers and KIT for the Helmholtz Young Investigators Group (Grant No. VH NG 734) and the TALISMAN Project (TALI C03 01) for funding. We also thank the KIT Synchrotron (previously ANKA) for the granted beamtime as well as the Radiation Protection officers for the assistance, and finally we thank the technicians of the CEA Atalante facility for the preparation of Pu glass samples.

REFERENCES

(1) Jantzen, C. M. Systems Approach to Nuclear Waste Glass Development. *J. Non Cryst. Solids* **1986**, *84*, 215−225.

(2) Vernaz, E.; Gin, S.; Veyer, C. Waste Glass A2. In *Comprehensive Nuclear Materials;* Konings, R., Ed.; Elsevier: Oxford, UK, 2012; pp 451−483.

(3) Ojovan, M. I.; Lee, W. E. Immobilisation of Radioactive Waste in Glass. In *An Introduction to Nuclear Waste Immobilisation,* 2nd ed.; Elsevier: Oxford, UK, 2014; pp 245−282.

(4) Kaushik, C. P. Indian Program for Vitrification of High Level Radioactive Liquid Waste. *Procedia Mater. Sci.* **2014**, *7*, 16−22.

(5) Ewing, R. C. Long term storage of spent nuclear fuel. *Nat. Mater.* **2015**, *14*, 252−257.

(6) Deissmann, G.; Neumeier, S.; Brandt, F.; Modolo, G.; Bosbach, D. In *Evaluation of the long term behavior of potential plutonium waste forms in a geological repository;* Materials Research Society Symposium Proceedings; Materials Research Society, 2014; pp 23−30.

(7) Kienzler, B.; Loida, A. *Endlagerrelevante Eigenschaften von hochradioaktiven Abfallprodukten. Charakterisierung und Bewertung. Empfehlung des Arbeitskreises HAW Produkte;* Forschungszentrum Karlsruhe: Kalrsruhe, Germany, 2001.
(8) Deschanels, X.; Peuget, S.; Cachia, J. N.; Charpentier, T. Plutonium solubility and self irradiation effects in borosilicate glass. *Prog. Nucl. Energy* **2007**, *49*, 623−634.
(9) Vienna, J. D.; Alexander, D. L.; Li, H.; Schweiger, M. J.; Peeler, D. K.; Meaker, T. F. *Plutonium dioxide dissolution in glass;* Pacific Northwest National Laboratory: Richland, WA, 1996.
(10) Feng, X.; Li, H.; Li, L. L.; Darab, J. G.; Schweiger, M. J.; Vienna, J. D.; Bunker, B. C.; Allen, P. G.; Bucher, J. J.; Craig, I. M.; Edelstein, N. M.; Shuh, D. K.; Ewing, R. C.; Wang, L. M.; Vance, E. R. *Ceram. Trans.* **1999**, *93*, 409.
(11) Schreiber, H. D.; Balazs, G. B. The Chemistry of Uranium in Borosilicate Glasses 0.1. Simple Base Compositions Relevant to the Immobilization of Nuclear Waste. *Phys. Chem. Glasses* **1982**, *23*, 139−146.
(12) Calas, G.; Galoisy, L.; Cormier, L.; Ferlat, G.; Lelong, G. The Structural Properties of Cations in Nuclear Glasses. *Procedia Mater. Sci.* **2014**, *7*, 23−31.
(13) Gin, S.; Jollivet, P.; Tribet, M.; Peuget, S.; Schuller, S., Radionuclides containment in nuclear glasses: an overview. In *Radiochim. Acta*, **2017**; Vol. *105*.10.1515/ract 2016 2658
(14) Krause, M. O.; Oliver, J. H. Natural Widths of Atomic K Levels and L Levels,K Alpha X Ray Lines and Several Kll Auger Lines. *J. Phys. Chem. Ref. Data* **1979**, *8*, 329−338.
(15) Vitova, T.; Kvashnina, K. O.; Nocton, G.; Sukharina, G.; Denecke, M. A.; Butorin, S. M.; Mazzanti, M.; Caciuffo, R.; Soldatov, A.; Behrends, T.; Geckeis, H. High energy resolution x ray absorption spectroscopy study of uranium in varying valence states. *Phys. Rev. B: Condens. Matter Mater. Phys.* **2010**, *82*, 235118.
(16) Pidchenko, I.; Kvashnina, K. O.; Yokosawa, T.; Finck, N.; Bahl, S.; Schild, D.; Polly, R.; Bohnert, E.; Rossberg, A.; Göttlicher, J.; Dardenne, K.; Rothe, J.; Schäfer, T.; Geckeis, H.; Vitova, T. Uranium Redox Transformations after U(VI) Coprecipitation with Magnetite Nanoparticles. *Environ. Sci. Technol.* **2017**, *51*, 2217−2225.
(17) Butorin, S. M.; Mancini, D. C.; Guo, J. H.; Wassdahl, N.; Nordgren, J.; Nakazawa, M.; Tanaka, S.; Uozumi, T.; Kotani, A.; Ma, Y.; Myano, K. E.; Karlin, B. A.; Shuh, D. K. Resonant X ray fluorescence spectroscopy of correlated systems: A probe of charge transfer excitations. *Phys. Rev. Lett.* **1996**, *77*, 574−577.
(18) Rothe, J.; Butorin, S.; Dardenne, K.; Denecke, M. A.; Kienzler, B.; Loble, M.; Metz, V.; Seibert, A.; Steppert, M.; Vitova, T.; Walther, C.; Geckeis, H. The INE Beamline for actinide science at ANKA. *Rev. Sci. Instrum.* **2012**, *83*, 043105.
(19) Vitova, T.; Denecke, M. A.; Göttlicher, J.; Jorissen, K.; Kas, J. J.; Kvashnina, K.; Prüßmann, T.; Rehr, J. J.; Rothe, J. Actinide and lanthanide speciation with high energy resolution X ray techniques. *Journal of Physics. J. Phys.: Conf. Ser.* **2013**, *430*, 012117.
(20) Kvashnina, K. O.; Butorin, S. M.; Martin, P.; Glatzel, P. Chemical State of Complex Uranium Oxides. *Phys. Rev. Lett.* **2013**, *111*, 253002.
(21) Butorin, S. M.; Kvashnina, K. O.; Vegelius, J. R.; Meyer, D.; Shuh, D. K. High resolution X ray absorption spectroscopy as a probe of crystal field and covalency effects in actinide compounds. *Proc. Natl. Acad. Sci. U. S. A.* **2016**, *113*, 8093−8097.
(22) Vitova, T.; Green, J. C.; Denning, R. G.; Löble, M.; Kvashnina, K.; Kas, J. J.; Jorissen, K.; Rehr, J. J.; Malcherek, T.; Denecke, M. A. Polarization Dependent High Energy Resolution X ray Absorption Study of Dicesium Uranyl Tetrachloride. *Inorg. Chem.* **2015**, *54*, 174−182.
(23) Vitova, T.; Pidchenko, I.; Fellhauer, D.; Bagus, P. S.; Joly, Y.; Pruessmann, T.; Bahl, S.; Gonzalez Robles, E.; Rothe, J.; Altmaier, M.; Denecke, M. A.; Geckeis, H. The role of the 5f valence orbitals of early actinides in chemical bonding. *Nat. Commun.* **2017**, *8*, 16053.
(24) Popa, K.; Prieur, D.; Manara, D.; Naji, M.; Vigier, J. F.; Martin, P. M.; Dieste Blanco, O.; Scheinost, A. C.; Prussmann, T.; Vitova, T.; Raison, P. E.; Somers, J.; Konings, R. J. M. Further insights into the chemistry of the Bi U O system. *Dalton T* **2016**, *45*, 7847−7855.
(25) Delaye, J. M.; Ghaleb, D. In *Glass: scientific research for high performance containment;* CEA/Valrhô Summer Session Proceedings, Méjannes le Clap, France, Aug 31−Sept 7; Méjannes le Clap, France, 1997; p 87.
(26) Cachia, J. N.; Deschanels, X.; Den Auwer, C.; Pinet, O.; Phalippou, J.; Hennig, C.; Scheinost, A. Enhancing cerium and plutonium solubility by reduction in borosilicate glass. *J. Nucl. Mater.* **2006**, *352*, 182−189.
(27) Pidchenko, I. Characterization of structural properties of U and Pu in model systems by advanced synchrotron based X ray spectroscopy. Dissertation, Karlsruhe Institute for Technology: Germany, 2016. doi: 10.5445/IR/1000054271.
(28) Zimina, A.; Dardenne, K.; Denecke, M. A.; Grunwaldt, J. D.; Huttel, E.; Lichtenberg, H.; Mangold, S.; Pruessmann, T.; Rothe, J.; Steininger, R.; Vitova, T. The CAT ACT Beamline at ANKA: A new high energy X ray spectroscopy facility for CATalysis and ACTinide research. *J. Phys.: Conf. Ser.* **2016**, *712*, 012019.
(29) Zimina, A.; Dardenne, K.; Denecke, M.; Doronkin, D.; Huttel, E.; Lichtenberg, H.; Mangold, S.; Pruessmann, T.; Rothe, J.; Spangenberg, T.; Steininger, R.; Vitova, T.; Geckeis, H.; Grunwaldt, J. D. *Review of Scientific Instruments.* Accepted for publication.
(30) Walshe, A.; Prussmann, T.; Vitova, T.; Baker, R. J. An EXAFS and HR XANES study of the uranyl peroxides [UO2(eta(2) O 2)(H2O)(2)]center dot nH(2)O (n = 0, 2) and uranyl (oxy) hydroxide [(UO2)(4)O(OH)(6)]center dot 6H(2)O. *Dalton T* **2014**, *43*, 4400−4407.
(31) Prüßmann, T. Characterization of bonding differences by advanced synchrotron based X ray spectroscopy. Doctoral Thesis, Karlsruhe Institute for Technology: Germany, 2016. doi: 10.5445/IR/1000052760.
(32) Ravel, B.; Newville, M. ATHENA, ARTEMIS, HEPHAESTUS: data analysis for X ray absorption spectroscopy using IFEFFIT. *J. Synchrotron Radiat.* **2005**, *12*, 537−541.
(33) Rehr, J. J.; Kas, J. J.; Vila, F. D.; Prange, M. P.; Jorissen, K. Parameter free calculations of X ray spectra with FEFF9. *Phys. Chem. Chem. Phys.* **2010**, *12*, 5503−5513.
(34) Hudry, D.; Apostolidis, C.; Walter, O.; Janssen, A.; Manara, D.; Griveau, J. C.; Colineau, E.; Vitova, T.; Prussmann, T.; Wang, D.; Kubel, C.; Meyer, D. Ultra Small Plutonium Oxide Nanocrystals: An Innovative Material in Plutonium Science. *Chem. Eur. J.* **2014**, *20*, 10431−10438.
(35) Conradson, S. D.; Begg, B. D.; Clark, D. L.; Den Auwer, C.; Espinosa Faller, F. J.; Gordon, P. L.; Hess, N. J.; Hess, R.; Keogh, D. W.; Morales, L. A.; Neu, M. P.; Runde, W.; Tait, C. D.; Veirs, D. K.; Villella, P. M. Speciation and unusual reactivity in PuO2+x. *Inorg. Chem.* **2003**, *42*, 3715−3717.
(36) Clark, D. L. The chemical complexities of plutonium. *Challenges in Plutonium Science* **2000**, *26*, 364−381.
(37) Burns, P. C.; Ewing, R. C.; Hawthorne, F. C. The crystal chemistry of hexavalent uranium: Polyhedron geometries, bond valence parameters, and polymerization of polyhedra. *Can. Mineral* **1997**, *35*, 1551−1570.
(38) Podkovyrina, Y.; Pidchenko, I.; Prüßmann, T.; Bahl, S.; Göttlicher, J.; Soldatov, A.; Vitova, T. Probing Covalency in the UO 3 Polymorphs by U M 4 edge HR XANES. *J. Phys.: Conf. Ser.* **2016**, *712*, 012092.
(39) Christoph, G. G.; Larson, A. C.; Eller, P. G.; Purson, J. D.; Zahrt, J. D.; Penneman, R. A.; Rinehart, G. H. Structure of barium plutonate by neutron powder diffraction. *Acta Crystallogr., Sect. B: Struct. Sci.* **1988**, *44*, 575−580.
(40) Morss, L. R.; Edelstein, N. M.; Fuger, J.; Katz, J. J. *The chemistry of the actinide and transactinide elements: Neptunium, Plutonium and Americium,* 3rd ed.; Springer: Dordrecht, The Netherlands, 2006; p 697.
(41) Loopstra, B. O. Neutron Diffraction Investigation of U3o8. *Acta Crystallogr.* **1964**, *17*, 651−654.

(42) Desgranges, L.; Baldinozzi, G.; Simeone, D.; Fischer, H. E. Structural Changes in the Local Environment of Uranium Atoms in the Three Phases of U4O9. *Inorg. Chem.* **2016**, *55*, 7485−7491.
(43) Hess, N. J.; Weber, W. J.; Conradson, S. D. X ray absorption fine structure of aged, Pu doped glass and ceramic waste forms. *J. Nucl. Mater.* **1998**, *254*, 175−184.
(44) Craw, J. S.; Vincent, M. A.; Hillier, I. H.; Wallwork, A. L. Ab Initio Quantum Chemical Calculations on Uranyl Uo22+ Plutonyl Puo22+, and Their Nitrates and Sulfates. *J. Phys. Chem.* **1995**, *99*, 10181−10185.
(45) Gaunt, A. J.; May, I.; Neu, M. P.; Reilly, S. D.; Scott, B. L. Structural and Spectroscopic Characterization of Plutonyl(VI) Nitrate under Acidic Conditions. *Inorg. Chem.* **2011**, *50*, 4244−4246.
(46) Buchsbaum, C.; Hahler Schlimm, S.; Rehme, S. Data Bases, the Base for Data Mining. *Struct. Bonding* **2009**, *134*, 37−58.
(47) Farges, F.; Ponader, C. W.; Calas, G.; Brown, G. E. Structural Environments of Incompatible Elements in Silicate Glass Melt Systems 0.2. Uiv, Uv, and Uvi. *Geochim. Cosmochim. Acta* **1992**, *56*, 4205−4220.
(48) Bahl, S. Advanced chemical and structural characterization of nuclear waste materials related to the nuclear fuel cycle. Doctoral Thesis, Karslruhe Institute for Technology: Germany, 2017.
(49) Servaes, K.; Hennig, C.; Billard, I.; Gaillard, C.; Binnemans, K.; Görller Walrand, C.; Van Deun, R. Speciation of uranyl nitrato complexes in acetonitrile and in the ionic liquid 1 butyl 3 methylimidazolium bis(trifluoromethylsulfonyl)imide. *Eur. J. Inorg. Chem.* **2007**, *2007*, 5120−5126.
(50) Taylor, J. C.; Mueller, M. H. A Neutron Diffraction Study of Uranyl Nitrate Hexahydrate. *Acta Crystallogr.* **1965**, *19*, 536−543.
(51) Stump, N. A.; Haire, R. G.; Dai, S. In *Spectroscopic investigations of neptunium's and plutonium's oxidation states in sol gel glasses as a function of initial valence and thermal history;* Materials Research Society Symposium Proceedings, 1997; pp 47−54. doi: 10.1557/PROC 465 47.
(52) Stefanovsky, S. V.; Shiryaev, A. A.; Zubavichus, Y. V.; Marra, J. C. In *Plutonium environment in lanthanide borosilicate glass;* Materials Research Society Symposium Proceedings, 2010; pp 21−26. doi: 10.1557/PROC 1264 Z11 09.
(53) Bouty, O.; Ramond, L.; Solari, P. L.; Cammelli, S. XANES analysis of a Cm doped borosilicate glass under alpha self irradiation effects. *J. Mater. Sci.* **2016**, *51*, 7918−7928.
(54) *Waste Acceptance Product Specifications (WAPS) For Vitrified High Level Waste Forms;* United States Department of Energy, 2012.
(55) Lumpkin, G. R. Ceramic waste forms for actinides. *Elements* **2006**, *2*, 365−372.
(56) Kienzler, B.; Loida, A.; Maschek, W.; Rineiski, A. Mobility and criticality of plutonium in a repository. *Nucl. Technol.* **2003**, *143*, 309−321.